Interaction of a Rectangular Jet with a Flat-plate placed parallel to the flow

K.B.M.Q. Zaman[1], C. A. Brown[2] and J. E. Bridges[3],

NASA Glenn Research Center
Cleveland, OH 44135

Abstract
An experimental study is carried out addressing the flowfield and radiated noise from the interaction of a large aspect ratio rectangular jet with a flat plate placed parallel to but away from the direct path of the jet. Sound pressure level spectra exhibit an increase in the noise levels for both the 'reflected' and 'shielded' sides of the plate relative to the free-jet case. Detailed cross-sectional distributions of flowfield properties obtained by hot-wire anemometry are documented for a low subsonic condition. Corresponding mean Mach number distributions obtained by Pitot-probe surveys are presented for high subsonic conditions. In the latter flow regime and for certain relative locations of the plate, a flow resonance accompanied by audible tones is encountered. Under the resonant condition the jet cross-section experiences an 'axis-switching' and flow visualization indicates the presence of an organized 'vortex street'. The trends of the resonant frequency variation with flow parameters exhibit some similarities to, but also marked differences with, corresponding trends of the well-known edgetone phenomenon.

1. Introduction

Driven by noise reduction goals, many newer aircraft concepts involve over-the-wing engine designs which provide a shielding effect for the jet exhaust noise propagated towards the ground. In many of these concepts rectangular geometries for the jet nozzle are preferred for ease of integration with the airframe and for possible noise benefits inherent to the non-axisymmetric geometry [1-3]. However, in many cases the jet exhaust just downstream of the nozzle is close to a surface before emanating as a free jet. In those cases jet-surface interaction becomes an important issue acoustically as well as aerodynamically. A research program was initiated in NASA to investigate these issues experimentally, computationally as well as analytically. Preliminary experiments were conducted in the Aeroacoustics Propulsion Laboratory (AAPL) at NASA Glenn Research Center (GRC) during May of 2012 with a round jet interacting with a flat plate [4]. Plans were developed for detailed future experiments with nonaxisymmetric nozzles in conjunction with various surface geometries.

An analytical effort was also under way by researchers at GRC [5]. The analysis was based on the assumption of two-dimensional (2-D) mean flows and for this effort a database was desired for a jet flow that was approximately two-dimensional and interacting with a flat surface. Because the schedule for the next phase of experiments in the AAPL was still many months away, it was decided that an experiment in a relatively smaller facility (test cell CW17 at GRC) be conducted in order to respond to this need in a timely manner. Catering to the 2-D constraints in the analysis a large aspect ratio (8:1) rectangular nozzle in combination with a flat-plate was chosen for the CW17 experiment. The nozzle and the plate were part of the same hardware to be used in the later AAPL experiment. The smaller facility was semi-anechoic and suited mainly for detailed flowfield data acquisition using various measurement techniques. Limited noise measurements were also possible. However, because of low operating costs this facility allowed fast parametric variations in order to explore various aspects of the problem at hand. Thus, the objective of the experiment was not only to provide a database for the analytical effort but also to provide parametric guidelines for the subsequent larger-scale experimental effort planned for the AAPL.

---

[1] Inlet & Nozzle Branch, Aeropropulsion Division, AIAA Associate Fellow.
[2] Acoustics Branch, Aeropropulsion Division, AIAA member.
[3] Acoustics Branch, Aeropropulsion Division, AIAA Associate Fellow.

Three tasks were carried out: (1) hot-wire surveys at a low Mach number, (2) Pitot-probe surveys primarily at a jet Mach number M_j =0.99 (acoustic Mach number M_a=0.90) and (3) far-field sound pressure level measurements covering a range of subsonic Mach numbers for both the reflected and the shielded sides of the plate. (With microphones overhead, the reflected and shielded sides represent plate locations underneath and over the jet, respectively.) The results obtained from this experiment are documented in this paper.

During the course of the experiment, an unexpected resonant interaction was encountered. It occurred in certain ranges of the parameters. In pronounced cases, it was accompanied by audible tones that obviously had an impact on the radiated noise. It is needless to say that an understanding of the resonant interaction is important not only to guide future research under the program but also so that it can be avoided or suppressed in possible future applications. The phenomenon was explored briefly with the given nozzle-plate combination and those results are also presented in this paper.

2. Experimental Facility and Procedure

The open jet facility housed in test cell CW17 at GRC, used for the current study, has been described in previous publications [6, 7]. Compressed air passes through a 30" diameter plenum chamber before exhausting through the nozzle into the ambient of the test chamber. Only cold (unheated) flow is available and flow visualization as well as detailed flow field surveys using hot-wire anemometry and Pitot-static probes are possible. The test cell has acoustic linings on the ceiling and upper walls and with proper preparation limited noise measurements, for assessing trends in relative changes in the noise characteristics, are possible; the quality of the noise data is discussed further in the following. With suitable transition sections, the same nozzles used in the AAPL can be investigated in this facility and vice versa. An 8:1 aspect ratio nozzle, referred to as 'NA8Z' in [8] and simply as 'R8' in the following, was adapted for the experiment. It was one of several nozzles that, in combination with different surface geometries, were to be studied in the later AAPL experiments. The design considerations for a class of rectangular nozzles including the R8 have been discussed in [8]; co-ordinates for the nozzle geometry can also be found in [6]. The nozzle exit had dimensions of 5.339"x0.658" and thus an equivalent diameter D=2.12". A half-inch thick 24"x12" aluminum plate was used as the interacting surface. The plate was placed parallel to the long edge of the nozzle, as illustrated in the photograph of the setup shown in Fig. 1(a). The plate had a 45˚ bevel on the trailing edge. Figure 1(b) shows a schematic of the setup together with the co-ordinate system used.

For the hot-wire measurements two X-wire probes, one in u-v and the other in u-w configuration, were used. For these data an auxiliary blower, capable of providing plenum pressures up to 1 psig, was used. Fluctuations in the plenum pressure during a survey (typically lasting about an hour) were within 0.5% of the set value. The photograph in Fig. 1(a) shows the plate aligned with the lower edge of the nozzle. Two X-wire probes can be seen just downstream and on the far side of the plate's trailing edge (TE). The plate is centered in the lateral direction (y) relative to the jet axis. The vertical (z) location of the plate was varied manually using a 'lab-jack'. The axial (x) location of the plate could also be varied manually in coarse steps. For a given axial plate-location, the hot-wire surveys were done at various x-stations; mean velocity and turbulence intensity data were acquired over the cross-sectional (y-z) plane. The surveys were repeated for various z-locations of the plate. All hot-wire results are for M_j =0.226 (same as in [6] that reported data for free jets from various rectangular nozzles including the R8). For nondimensionalization of the data the equivalent diameter D and the jet velocity U_j are used. Unless stated otherwise all data presented in this paper pertain to an axial location of the plate such that its TE was at x_{TE}/D=5.66 with the leading edge located at the nozzle exit plane.

A rake of three Pitot probes was used for the surveys at higher jet Mach numbers. The spacing of the probes in the y direction was 0.48" and this was the spatial resolution in that direction for all Pitot probe surveys. Jet Mach numbers ranging from 0.5 to slightly over 1.0 were tested; most of the data were for M_j =0.99. Surveys were conducted at the same x-stations and plate z-locations as covered with the hot-wire data. The pressures

read by the three probes were cross-checked by placing the rake in a region of uniform flow at the exit of the nozzle and corrections were made for small mismatch in calibrations. For the Pitot surveys air supply from the 'central control' of GRC was used. During the surveys, even though the plenum pressure was held by automated feedback control, fluctuations occurred depending on other users of the central control air supply and this contributed to the largest uncertainty in the plenum pressure. However, the Mach number data were normalized by the 'current' jet Mach number (M_j) calculated from the plenum pressure (p_0) read simultaneously with the Pitot data. The rms fluctuation in M_j (in percent of average M_j) over an entire run was calculated and indicated with all data sets. The jet Mach number was calculated from the nozzle pressure ratio as, $M_j = (((p_0 / p_a)^{(\gamma-1)/\gamma} - 1)\frac{2}{\gamma-1})^{1/2}$, where p_a is the ambient pressure and γ is the ratio of specific heats for air.

Four ¼-inch (B&K 4135) microphones held fixed on an overhead arm were used for the noise measurements. The actual polar locations and corresponding distances from the exit of a 2" diameter round nozzle are listed in the table below. The round nozzle was used to check repeatability of the noise data. Here, θ is measured with respect to the jet's downstream axis. The R8 nozzle was longer and its exit was located 4" downstream relative to the exit of the round nozzle. Thus the angular locations and distances are somewhat different, as also listed in the table. For simplicity, the angular locations for the four microphones are referred to in the following by the nominal values of 25˚, 60˚, 75˚ and 90˚, respectively.

Table 1 Microphone locations relative to 2" diameter round nozzle and R8 nozzle.

Mic #	Polar location, θ (deg)	Distance, r (in)	Nozzle
1	26.2	85.8	Round
2	61.2	51.6	Round
3	74.7	48.75	Round
4	90.0	48.75	Round
1	27.5	82.3	R8
2	66.0	50.1	R8
3	79.5	47.9	R8
4	95.0	48.9	R8

The spectrum analysis was done over 0-50kHz with a bandwidth of 125.0 Hz. For some of the data, a narrower analysis range (0-10kHz) was used with a bandwidth of 25Hz. The quality of the noise data is discussed in §3.3. In the spectral plots the nominal polar location, jet Mach number and OASPL are shown in the second, third and fourth columns of the legend, respectively. The measurements on the reflected side were done with the configuration shown in Fig. 1(a). The configuration shown in Fig. 1(c) was used for noise measurement on the shielded side of the plate.

3. Results

3.1 Hot-wire surveys: As stated earlier, all hot-wire data in the following pertain to M_j =0.226 and unless stated otherwise all data in this paper are for an axial location of the plate with trailing edge at x_{TE}/D=5.66. Figure 2 shows the mean streamwise velocity measured just downstream of the plate's TE (x/D=5.75). Data for three z-locations of the plate are shown. The distribution in Fig. 2(a) is for the case when the plate is flush with the lower edge of the nozzle. With the confinement imposed by the plate the jet is forced to spread in the lateral (y) direction and vortical (turbulent) flow could be detected as far as $y/D \approx 2$. In comparison, for plate location z/D = -0.5 in Fig. 2(b), there is room for the jet to spread in the negative z-direction. As a result the lateral spread is not as much and also the peak

velocities in the core have fallen significantly. The trend continues with farther spacing of the plate, z/D = -1, in Fig. 2(c). In [6] data for the free jet from this nozzle was reported for various x-locations. In Fig. 3, the distribution at x/D=8 from the cited reference is compared with the present measurements for a plate location z/D = -2.75. There is little difference between the two data sets and this indicates a negligible effect on the mean flow for the given plate spacing. In fact, the effect of the plate appeared negligible even for z/D = -1.5 (corresponding mean velocity distribution, not shown for brevity, appeared similar to that in Fig. 3a with only small differences on the lower side of the jet).

Turbulence intensity distributions corresponding to the cases of Fig. 2 are presented in Fig. 4. Higher peak intensity is noted for the smallest separation of the plate in Fig. 4(a). For this case the flow is essentially a wall jet and exhibits a single band of high intensity; (the boundary layer on the plate surface is not resolved in these measurements). With z/D= -1 (Fig. 4c), on the other hand, a lower and an upper band of high intensity can be seen. This is commensurate with expected trend in a free jet where two such bands occur in the upper and lower shear layers. A few other turbulent quantities, for plate location z/D = -1, are shown in Fig. 5. The transverse (vertical) component of turbulence intensity (w', Fig. 5a) has a much lower peak level relative to that of the axial component u' (about 0.10 versus 0.135; Fig. 4c). Such anisotropy in the turbulence field was also noted for the free jet [6]. While it is not shown in Fig.5, the lateral component of the intensity (v') has a distribution and peak level similar to those of w' in Fig. 5(a). The transverse Reynolds stress component (uw, Fig. 5b) exhibits a distribution as expected; the positive and negative regions on the top and bottom are commensurate with corresponding U-gradients with opposite signs. The lateral Reynolds stress component (uv), on the other hand, has a more complex distribution. The negative region at the top indicates lateral momentum transfer by the turbulent field away from the center. The positive region on the right indicates inward momentum transfer. These turbulent quantities are documented in order to aid computational as well as analytical efforts. It is clear by now that the assumption of two-dimensionality for the flow should be used with caution and it may be applicable only in the central portion of the flow-field.

3.2 Pitot probe surveys at higher M_j:

Figure 6 presents contours of Mach number, normalized by the respective jet Mach number, just downstream of the plate TE for plate location z/D = -2.75; data for three M_j are shown. Essentially the same distributions are noted in the three plots. From the legends it can be seen that the peak value within the field increases somewhat with increasing M_j, indicating a lengthening of the jet's development region with increased compressibility at higher M_j. In Fig. 7, the jet cross section at the same x-station (x/D=5.75) is shown for M_j =0.99, with variation of the z-location of the plate. For z/D = -0.155 (plate touching the lower edge of the nozzle, Fig. 7a), a similar distribution may be noted as seen with the hot-wire data for incompressible flow (Fig. 2a). For plate location z/D = -1.5 (Fig. 7d) the effect of the plate on the flow field appears insignificant. The contours are similar to those seen in Fig. 6 for z/D = -2.75, indicating a free-jet-like behavior. For the intermediate z-locations, an interaction is evident. For z/D = -0.5 (Fig. 7b), there is a pronounced outward bowing of the jet core. For z/D = -1.0 (Fig. 7c), the distribution is quite different from what was seen with the hot-wire data at low M_j (Fig. 2c); the middle of the jet cross-section here exhibits a distinct outward stretching in the vertical (z) direction.

At high M_j and for z/D = -1.0 there was a perceptible tone emitted from the flow, as demonstrated later with the noise spectra. The tone frequency (f_p) was about 1100 Hz corresponding to a Strouhal number ($f_p\, D/U_j$) of about 0.18. Thus, there was a naturally occurring periodic forcing of the jet. Such forcing caused the jet to go through an 'axis switching'; Fig. 7(c) caught this process at an intermediate stage where the switching had not yet completed. The entire process is illustrated by data at a few other x-stations shown in Fig. 8. By x/D=12, the axis switching is complete and the jet's major axis has become vertical.

The axis switching phenomenon was investigated in [9]. Evidence was shown that the switching could occur by two different vortex dynamics. One was due to the action of streamwise vortex pairs (e.g., introduced by tabs/chevrons). These were vortices with a steady state definition and their effect on axis switching was quite pronounced. The other, pertinent to the present case, was due to the dynamics of the unsteady azimuthal vortical structures. A periodic forcing would make the sheet of azimuthal vorticity emanating from the nozzle roll up into

discrete vortex 'rings' (with initial shape determined by the geometry of the nozzle exit). The non-axisymmetric vortex rings would go through self-induced contortions that would also lead to axis switching. The key was the roll-up of the azimuthal vorticity into the nonaxisymmetric rings. This may sometimes occur naturally, e.g., at low Reynolds numbers when the efflux boundary layer is laminar and susceptible to naturally occurring disturbances. Periodic perturbations, e.g., naturally occurring screech phenomenon or artificial perturbation, would also yield the same effect. Without such periodic perturbation the axis switching was seldom observed at higher jet Reynolds number and Mach number. These notions were substantiated by data from rectangular nozzles reported in the cited reference; at subsonic conditions there was no axis switching whereas a pronounced axis switching occurred at supersonic conditions when there was screech. Furthermore, the frequency of the perturbation needed to be around the 'preferred mode' Strouhal number where the jet would be most susceptible to the forcing. These observations are also borne out by the data presented here. The tone was most pronounced in a small range of M_j around 0.95 when clear axis switching occurred (Fig. 8c). At a lower or higher M_j, the tone around 1100Hz was either weak or disappeared (shown further with the noise spectral data in the following). Under the no- or weak-tone conditions at M_j =0.87 and 1.05 there was no axis switching, as can be inferred from the roughly round shape of the jet cross-section measured at the same axial station (x/D=12), shown in Figs. 9(a) and (b).

3.3 Noise field measurements:

As indicated earlier, the test chamber (CW17) was not ideal for noise measurements. However, precautions were taken by wrapping exposed surfaces near the nozzle with sound absorbing material. In [7] data for free round jets from this facility were compared with data from other facilities including the AAPL. It was noted that about 2dB scatter existed from facility to facility for shallow angles. The analysis in [5] mostly considers data at 90 degrees where the scatter is somewhat greater. Comparison of noise data for free jets from the R8 nozzle between the CW17 and the AAPL facilities exhibit even greater differences. This is shown in Fig. 10 for M_j =0.968 with data taken on the minor axis of the nozzle. The lower pair of traces is for θ=90˚with scale on the right while the upper pair is for θ=25˚ with scale on the left. The spectra from CW17 have somewhat different shapes and the levels are about 4 dB higher in certain frequency ranges at 90˚ as well as at 25˚. The ambient temperature and relative humidity were different in the two tests (70˚F and 40% in CW17 versus 34.5˚F and 76% in the AAPL), however, these differences may not impact the comparison since jet noise scales primarily with Mach number which was kept the same. It is possible that part of the difference stemmed from differences in the relative distance of the microphones; (for θ=90˚ only at 23D in CW17 versus 71D in the AAPL). Perhaps, the noisier minor axis plane is even more noisy closer to the nozzle. Furthermore, it has been shown that the spectral shape for a given (round) nozzle varies if the measurement location is too close. For example, at θ=25˚ and comparable M_j, levels higher by about 2 dB occur at high frequencies when the measurement location is moved from 50D to 30D [10]. It is not clear but some of these factors might have contributed to the less favorable comparison of the noise spectra for the R8 nozzle between the two facilities. In any case, higher levels in the CW17 facility are expected because of non-anechoic conditions and for reliable absolute spectral magnitudes one should use the data from the AAPL experiments. (Note that the round nozzle used in [7] had a diameter of 1.47", as opposed to 2.12" for the R8 nozzle, and thus the relative locations of the microphones were farther. Here, an additional note of caution is in order for the current noise measurement on the shielded side of the plate. First, because of the finite dimensions of the plate, noise could travel around it and thus this side was not truly 'shielded'. Second, referring back to Fig. 1(c), it can be seen that there are two posts holding the plate and a surface underneath that are in the vicinity of the jet. Even though these are wrapped with sound absorbing material their proximity may have influenced the noise spectra. A better arrangement would be to support the plate from above with minimal intrusions in the acoustic field. This will be done in the later experiment in the AAPL.)

It should be borne in mind that the differences in the spectra discussed above are from facility to facility. For a given facility, the data were repeatable within a much tighter scatter band. At the start of the present experiment in CW17 the repeatability of the spectra for a free jet was checked with a 2" diameter round nozzle for which earlier sets of data existed. The comparison with the earlier data was excellent; the scatter in

OASPL was within 0.3 dB. Thus, for a study of comparative levels ('deltas') and their general trends the data from the CW17 facility are thought to be acceptable.

In the following, SPL spectra are presented as measured without any correction or normalization. The spectral traces on the reflected and shielded sides are compared with free jet data in Figs. 11-13. Figure 11 compares the spectral data for plate locations, z/D= ±0.5, ±1.0 and ±1.5, with x_{TE}/D=5.66 and for θ= 90˚ and M_j =0.99. It can be seen that the noise levels are larger for either reflected or shielded sides on the low-frequency end, relative to the free jet case. The main difference between the reflected and shielded sides occurs on the high-frequency end; the former side, as expected, is noisier. Note the peak at about 1100 Hz for plate location z/D= ±1 (Fig. 11b). This is the resonant tone that caused the axis switching (§3.2). The amplitudes at the peak and neighboring frequencies are larger on the reflected side. Note that when there is a strong tone, 'broadband noise amplification' occurs and levels at other frequencies are also increased.

Figure 12 shows corresponding spectral data for the tone case (z/D=±1.0, M_j = 0.99) at three other polar locations. Similar trends are observed as seen for θ=90˚ (Fig. 11b). However, the tone is most prominent in the mid-polar locations (θ=60˚ and 75˚). In Fig. 13, data for plate location of z/D = ±1.0 are compared for two other jet Mach numbers. The tone at 1100 Hz (seen for M_j =0.99) has disappeared at both the higher or lower M_j. Recall that at these conditions the jet also does not undergo axis switching (Fig. 9). At M_j =1.055 (Fig. 13b) there is a screech component at just over 10kHz. This is seen with either plate location as well as for the free jet. The corresponding Strouhal number (about 1.8) is far removed from the 'preferred mode' Strouhal number; (the nominal value for the latter is 0.3 in incompressible flow and likely to be somewhat lower at higher Mach numbers). As a result, the screech in this case fails to produce energetic vortex rings that would persist in the flow and cause the axis switching.

3.4 Further data on the flow resonance:

The resonance phenomenon was explored further with the given plate. The spectral data in the following are shown only for the angular location of 60˚ and are taken with a narrower bandwidth so that the spectral peaks could be discerned clearly. In Fig. 14, SPL spectra are shown for varying z location of the plate, for M_j =0.98 and x_{TE}/D =5.66. It can be seen that a peak at about 1800Hz occurs for z/D= -0.71; this peak persists at lower values of z too, although the amplitude is barely greater than the broadband levels. At larger values of z, a jump occurs to a lower frequency. The spectral peak at the latter frequency (about 1100 Hz) persists up to about z/D= -1.42 and disappears at even larger z.

The dependence of the tone on M_j is illustrated in Fig. 15, for x_{TE}/D =5.66 and z/D= -1.0. The spectral peak is noticed over the entire M_j range covered (0.752 – 1.072), however, it is most prominent in the middle of the range. Furthermore an increase in the tone frequency with increasing M_j can be noticed. From M_j =0.795 to 1.013, the frequency has increased from 1010Hz to 1130Hz. Figure 16 shows corresponding data for M_j =0.99 as the plate is translated axially. The plate TE location is indicated for each spectral trace. At each axial location, the plate was moved in z until the tone was prominent. It was found that the spectral peak was weak or not detectable outside of the x_{TE}/D range covered in Fig. 16. For x_{TE}/D =4.25 there is a clear peak accompanied by a loud tone at 1725Hz.With increasing axial distance the frequency decreases continuously until at about x_{TE}/D =4.72 a lower frequency peak becomes dominant; thus, there is a 'stage jump'. Note that the lower frequency peak was also present at lower values of x_{TE} albeit with smaller amplitudes. With further increase in x_{TE} the tone frequency decreases again. From x_{TE}/D =4.72 to 6.13 the frequency dropped from 1250 to 1050 Hz.

Schlieren flow visualization pictures are shown in the following. First, data for varying z location of the plate with x_{TE}/D =5.66 and M_j =0.96 are presented in Fig. 17. The four z-locations of the plate in this figure correspond to those for which the cross-sectional Mach number contours near the TE were shown in Fig. 7. Note that for z/D= -0.155 and -0.5 the jet basically hugs the plate surface. At z/D= -1, however, there is an undulation in the jet column. This is the condition when the peak in the spectra occurs and the flow field goes through the axis switching. For z/D= -1.50 the path of the jet again becomes straight, commensurate with the disappearance of the resonance.

Figure 18 shows the flowfield for two TE locations of the plate for which the resonance was the most pronounced. These data are for M_j =0.96 with plate lateral location z/D= -0.71. The undulations suggest the presence of alternate vortices with opposite signs on the upper and lower sides of the jet. The vortex on the lower side hugs the plate surface. It is likely that the passage of the lower vortex train past the trailing edge creates pressure pulses that complete the feedback loop to sustain the resonance.

The suggested feedback mechanism is similar to that occurring in classical edgetone phenomenon. The latter phenomenon with rectangular jets and a wedge placed at the centerline of the flow has been studied over many decades in the past. In Fig. 19, the frequencies of the tone (from Fig. 16) are plotted as a function of x_{TE}/D. Only data points corresponding to clearly discernible peaks are chosen. A decreasing frequency with increasing x_{TE} can be seen. Also clear is the stage jump around x_{TE}/D =4.6. The data are compared with classic edgetone frequency variation using equations provided in [11]. For the latter phenomenon, the various stages are characterized by the number of vortices fitted between the nozzle exit and the leading edge of the wedge. (The locations of the stage jumps and the extent of the hysteresis loops in Fig. 19 are shown arbitrarily.) The present data do show a resemblance with the trend for the edgetone insofar as the frequency in each stage decreases with edge distance from the jet. Perhaps, the TE of the plate in the present case has a role similar to the leading edge of the wedge in the latter case. However, frequency variations do not clearly match the edgetone curves and there is another obvious contrast. While with increasing standoff distance a stage jump occurs to a higher frequency in edgetone, here a jump to a lower frequency has taken place. At this point, the mechanism of the resonance phenomenon remains far from clearly understood; this will be the focus of future efforts.

4. Conclusions

The flow and noise fields for an 8:1 aspect ratio rectangular jet interacting with a flat plate are presented in this paper. The rectangular nozzle has exit dimensions of 5.34x0.658 inches and the ½ inch thick plate has dimensions of 24x12 inches. With the plate centered in the spanwise direction with respect to the long edge of the nozzle, the axial and lateral distances of the plate are varied. For variations of these parameters as well as Mach number, the flow and noise field characteristics are explored. Noise is measured with microphones overhead for either the lower or the upper locations of the plate relative to the jet. All flow field data are acquired with the plate located below the jet. Sound pressure level spectra exhibit an increase in the noise levels for both the reflected and shielded sides of the plate. Cross-sectional distributions of mean velocity and turbulence intensity obtained by hot-wire anemometry are documented for a low subsonic condition. Corresponding Mach number distributions at high subsonic conditions are obtained by Pitot probe surveys. Some of these data are being used for comparison with an ongoing analytical study.

For certain locations of the plate a flow resonance accompanied by an audible tone is observed at high subsonic conditions. Under such resonant condition the jet cross-section goes through an axis-switching, i.e., the jet cross section which is initially elongated in the horizontal direction becomes elongated in the vertical direction after a certain downstream distance. In contrast, the jet cross-section gradually becomes round with increasing downstream distance for non-resonant conditions. Flow visualization indicates the presence of an organized ‘vortex street’ in the flow. Apparently opposite sign vortices are formed above and below the jet column in a staggered manner. The train of vortices underneath hugs the plate surface. The interaction of these vortices with the trailing edge of plate likely sustains the resonance. The characteristics of the frequency variation of the resonance has some similarities with the well-known edgetone phenomenon. However, there are also marked differences and the feedback loop responsible for sustaining the resonance remains from being clearly understood. Obtaining a correlation of the frequency variation with geometric and flow parameters and advancing the understanding of the mechanism will be the focus of further experiments in the near future.

Acknowledgement

Thanks are due to Dr. Amy Fagan and Michelle Clem of NASA GRC for help with obtaining the Schlieren flow visualization pictures. Support from The Fixed Wing Project of NASA's Fundamental Aeronautics Program is gratefully acknowledged.

References:

[1] Bridges, J.E., "Noise of embedded high-aspect ratio nozzles", presented at the NASA Fundamental Aeronautics Program 2011 Technical Conference, Cleveland, OH, March 15-17, 2011.
[2] Balsa, T.F., Gliebe, R.R., Kantola, R.A., Mani, R., Stringas, E.J. and Wang, J.C.F., "High velocity jet noise source location and reduction, Task 2 – theoretical developments and basic experiments", *Report No. FAA-RD-76-79, II*, General Electric Co., Aircraft Engine Group, Cincinnatti, OH, May, 1978.
[3] Massey, K.C., Ahuja, K.K. and Gaeta, R., "Noise Scaling for Unheated Low Aspect Ratio Rectangular Jets", *AIAA paper 2004-2946*, 10th AIAA/CEAS Aeroacoustics Conference, Manchester, England 10-12 May 2004.
[4] Brown, C. A., "Jet-surface interaction test: far-field noise results", *Proc. ASME Turbo Expo 2012*, GT2012, June 15-19, Copenhagen, Denmark, 2011.
[5] Afsar, M., Goldstein, M.E. & Leib. S. J., "Prediction of low-frequency trailing edge noise using rapid distortion theory", to be presented at the 14th European Turbulence Conference, Lyon, France, Sept 1-4, 2013.
[6] Zaman, K.B.M.Q., "Flow-field surveys for rectangular nozzles", *NASA TM-2012-217410* (see also *AIAA Paper 2012-0069*), 2012.
[7] Zaman, K.B.M.Q. and Dahl, M.D., "Noise and spreading of subsonic coannular jets – comparison with single equivalent jet", *AIAA J.*, 45(11), pp. 2661- 2670, 2007.
[8] Frate, F.C. and Bridges, J.E., "Extensible rectangular nozzle model system", *AIAA Paper 2011-975*, 49th Aerospace Sciences Meeting, Orlando, Fl, 4-7 January, 2011.
[9] Zaman, K.B.M.Q., "Axis switching and spreading of an asymmetric jet: the role of coherent structure dynamics", *J. Fluid Mech., 316*, pp. 1-27, 1996.
[10] Koch, L.D., Bridges, J.E., Brown, C.A. and Khavaran, A., "Experimental and analytical determination of the geometric far field for round jets", *Noise Control Engr. J.*, vol. 53, no. 1, pp. 20-28, 2005.
[11] Brown, G.B., "The vortex motion causing edge tones", *Proc. Physical Society* (London), vol. 49, pp. 493-507, 1937.

(a)

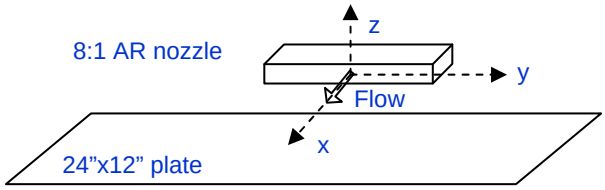

(b)

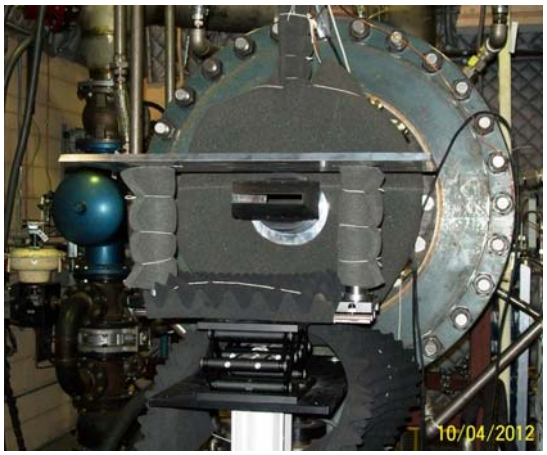

(c)

Fig. 1 Experimental setup. The 8:1 aspect ratio nozzle (R8) has 5.339”x0.658” exit. (a) Configuration with 24”x12” plate below nozzle (here, aligned with nozzle’s lower edge), (b) schematic of setup with co-ordinates, (c) configuration with plate above nozzle for noise measurement on shielded side.

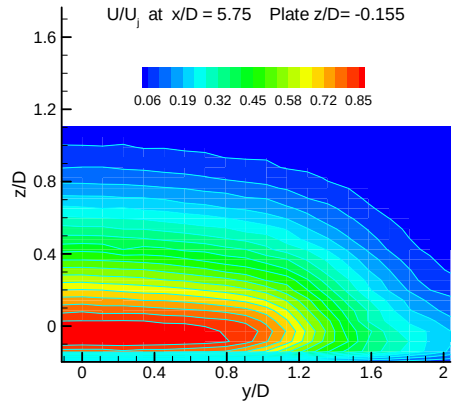

(a)

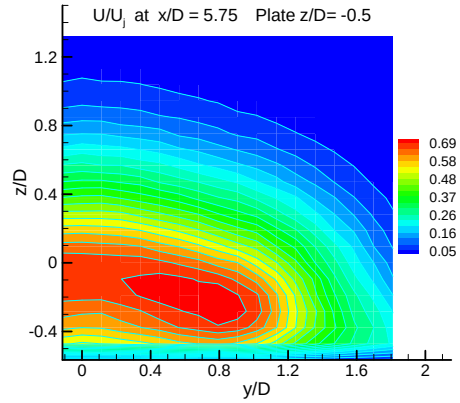

(b)

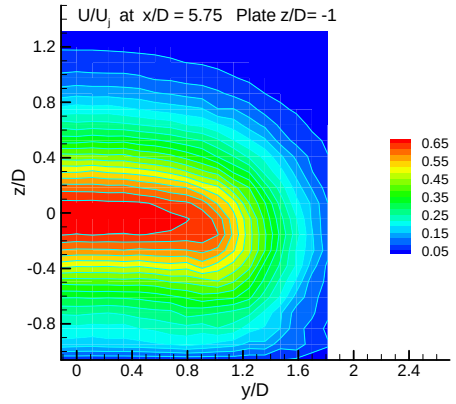

(c)

Fig. 2 Mean velocity distribution just downstream of plate’s TE (x/D=5.75), M_j = 0.226. Plate’s z-locations: (a) z/D = -0.155 (aligned with nozzle’s lower edge), (b) z/D = -0.5 and (c) z/D = -1. (Axial location of plate’s TE, x_{TE}/D=5.66 in all figures in the following unless stated otherwise.)

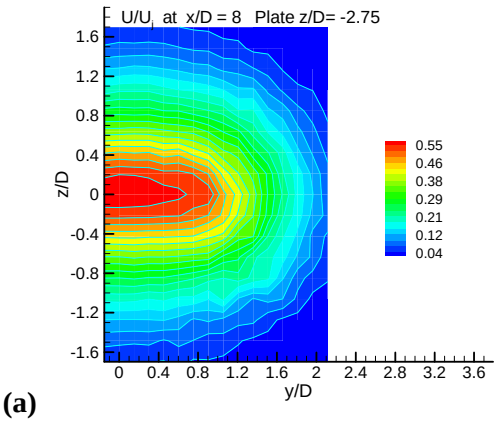

(a)

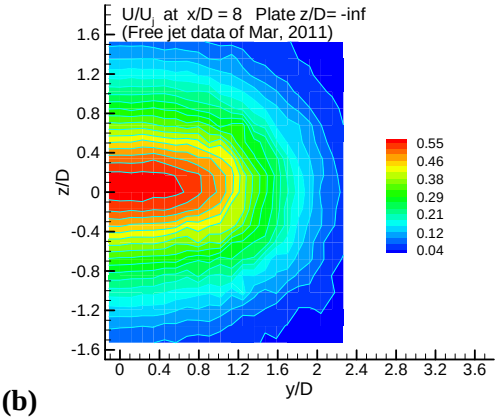

(b)

Fig. 3 Mean velocity distribution at *x/D*=8; M_j =0.226. (a) Plate at *z/D* = -2.75, (b) free-jet without plate (data from [6]).

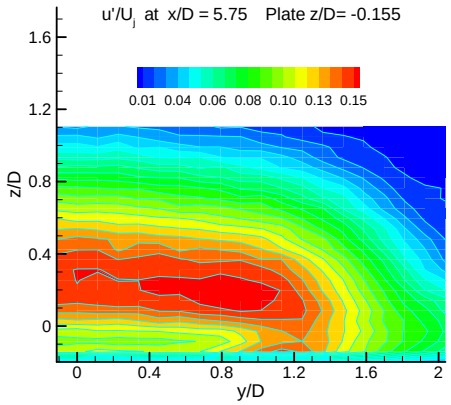

(a)

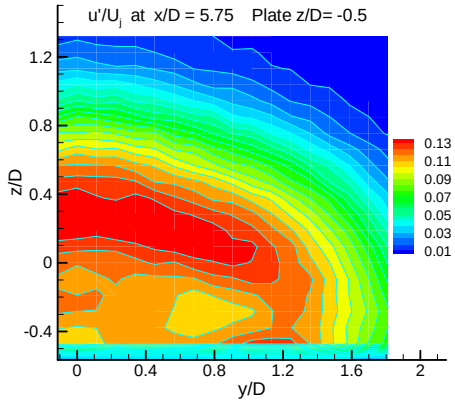

(b)

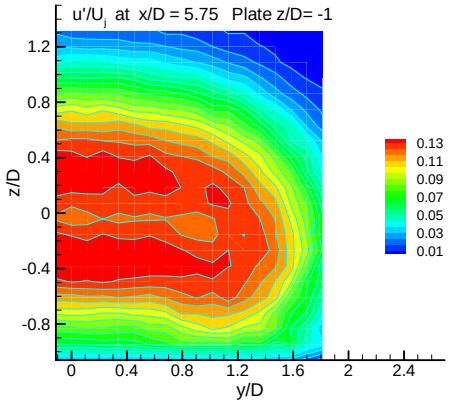

(c)

Fig. 4 Turbulence intensity (u'/U_j) distributions corresponding to mean velocity data of Fig. 2.

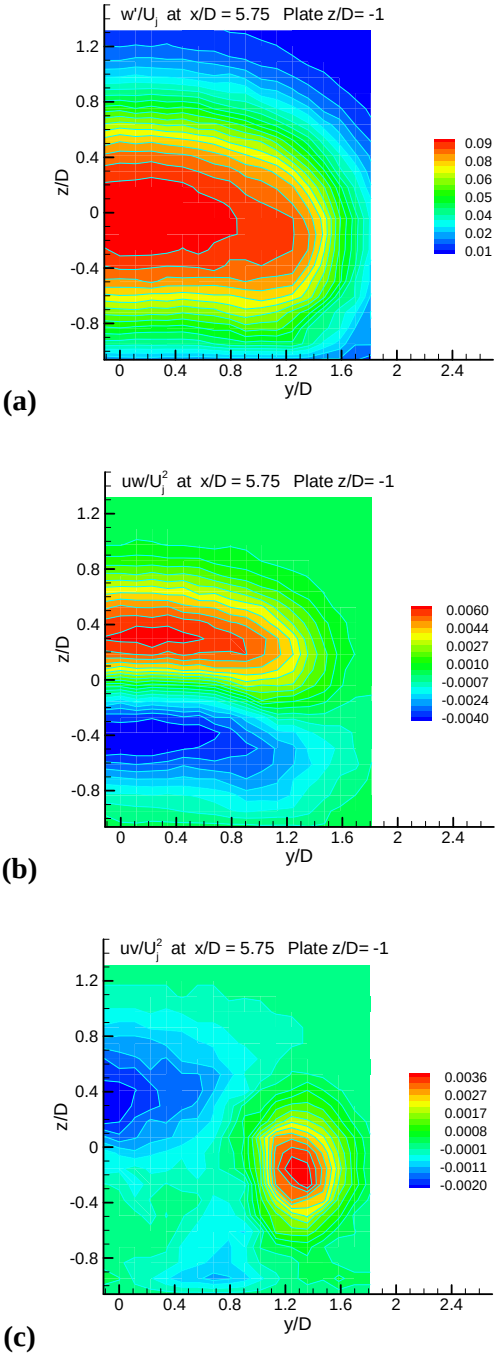

Fig. 5 Other turbulent stress components at *x/D*=5.75 for plate location *z/D* = -1 (corresponding to Figs. 2c and 4c); (a) w'/U_j, (b) uw/U_j^2 and (c) uv/U_j^2.

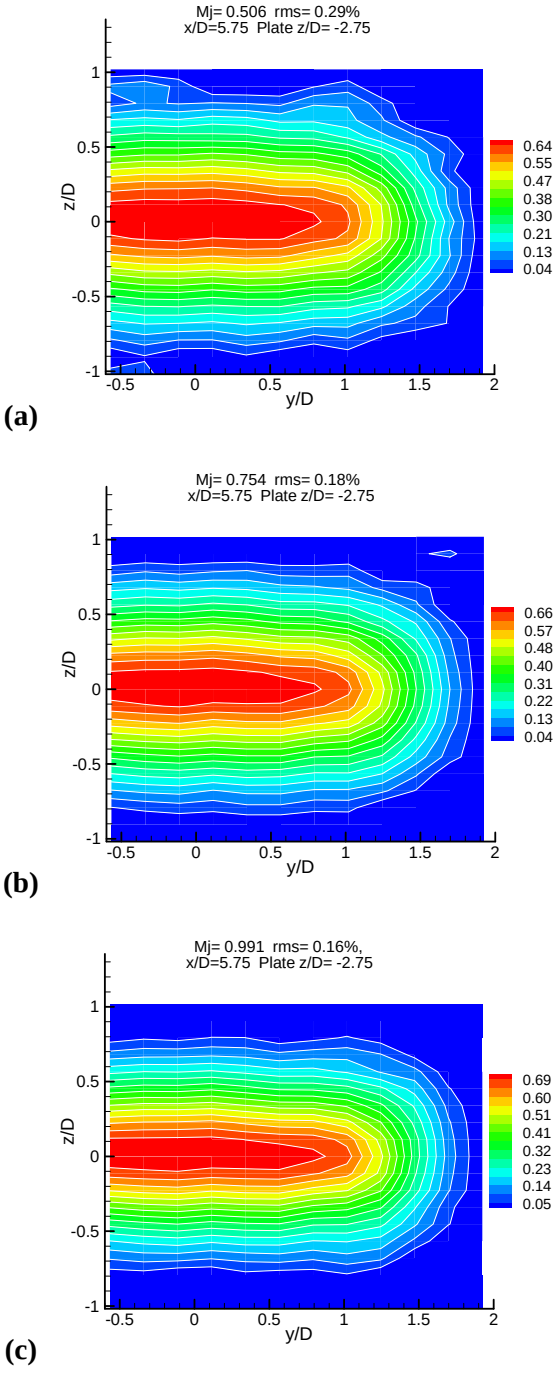

Fig. 6 Mach number (M/M_j) contours at *x/D*=5.75 obtained by Pitot probe surveys. Data are for 3 different M_j with plate at *z/D* = -2.75: (a) M_j = 0.5, (b) M_j = 0.75 and (c) M_j = 0.99.

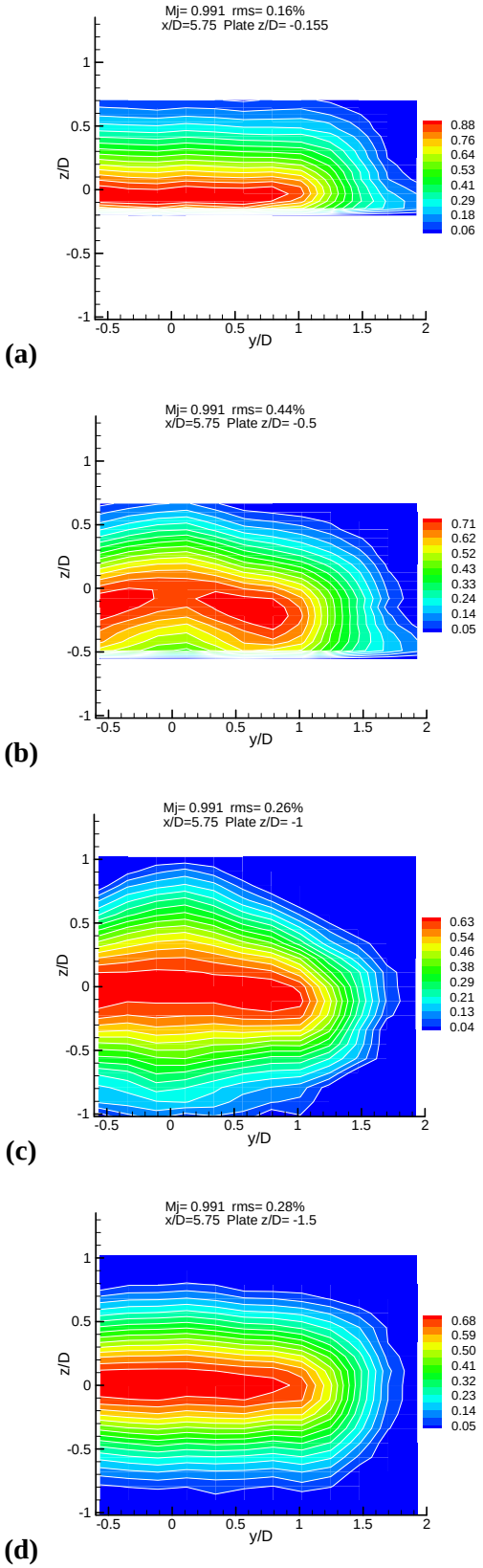

Fig. 7 M/M_j contours at x/D=5.75 for M_j =0.99. Plate z/D: (a) -0.155, (b) -0.5 , (c) -1 and (d) -1.5

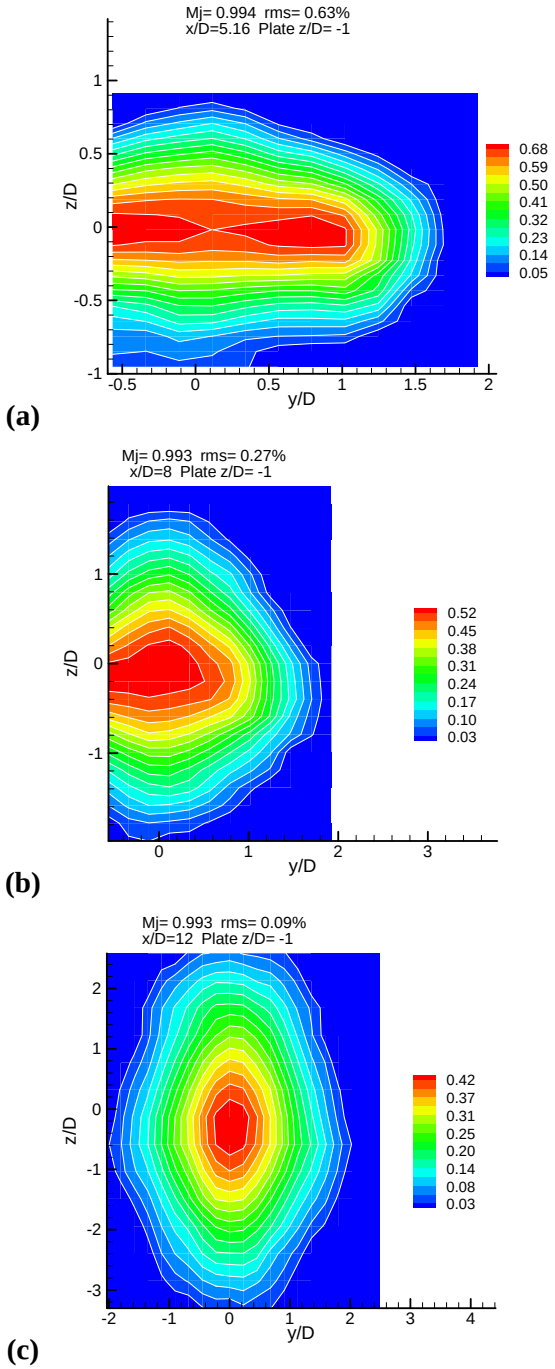

Fig. 8 M/M_j contours at three x-stations illustrating 'axis switching'; plate z/D =-1, M_j =0.99. (a) x/D = 5.16 (over plate), (b) x/D = 8 and (c) x/D=12. Corresponding data at x/D=5.75 in Fig. 7(c).

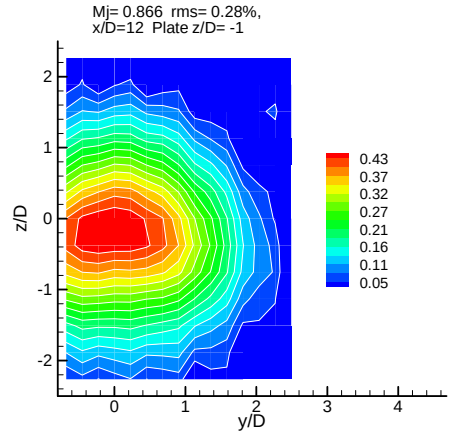

(a)

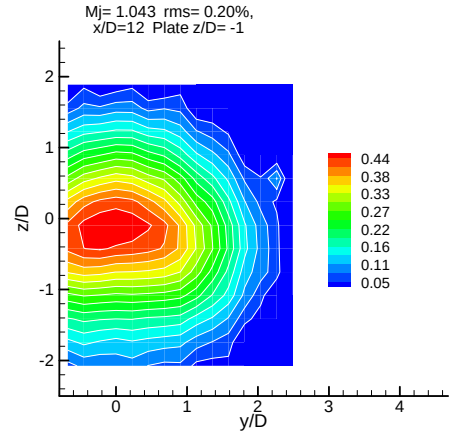

(b)

Fig. 9 M/M_j contours at x/D=12 with plate z/D = -1 for two other M_j: (a) M_j = 0.87, (b) M_j = 1.04.

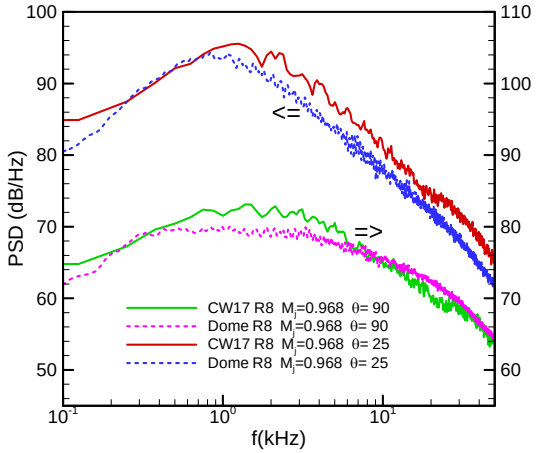

Fig. 10 Comparison of power spectral density of SPL for free-jet from the R8 nozzle measured in CW17 and AAPL (Dome) facilities; data referenced to one-foot distance from nozzle.

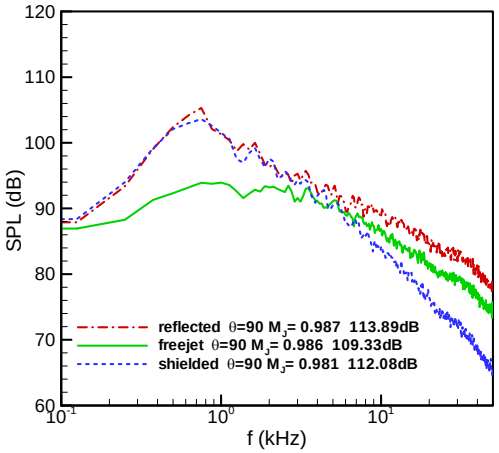

(a)

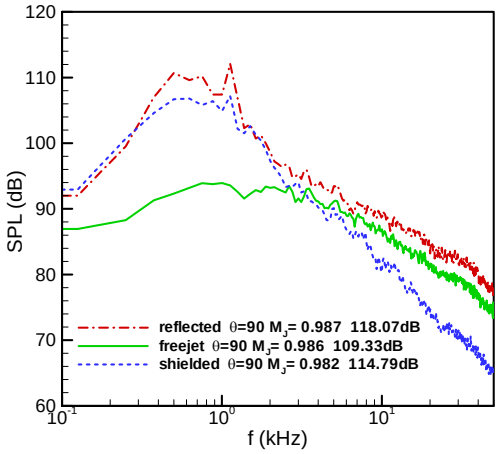

(b)

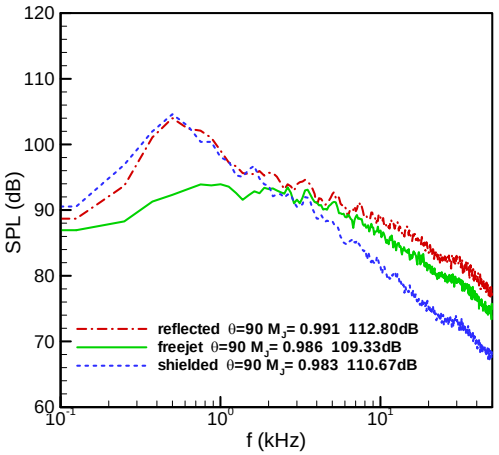

(c)

Fig. 11 SPL spectra at θ=90˚ for reflected and shielded sides of plate compared to free jet data; M_j = 0.99. Plate z/D: (a) ±0.5, (b) ±1.0 and (c) ±1.5.

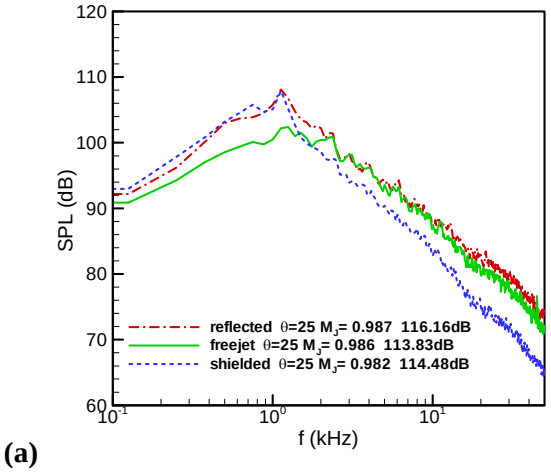

(a)

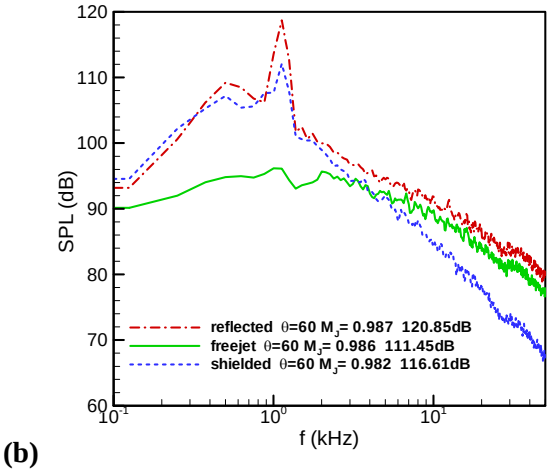

(b)

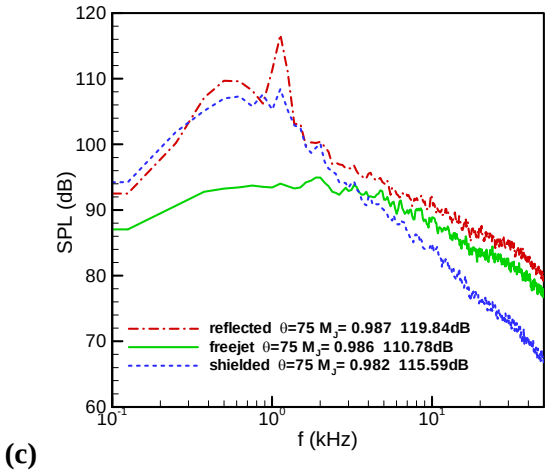

(c)

Fig. 12 SPL spectra for plate z/D =±1.0 for reflected and shielded sides compared to free jet data; M_j = 0.99. Microphone locations (θ): (a) 25˚, (b) 60˚ and (c) 75˚.

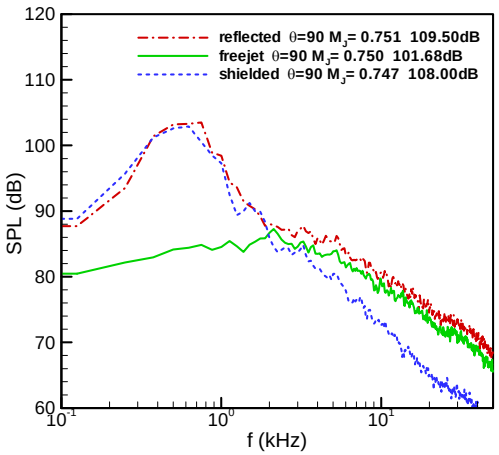

(a)

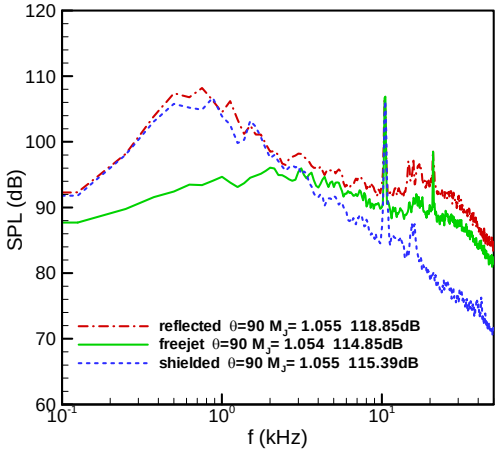

(b)

Fig. 13 SPL spectra at θ=90˚ on reflected and shielded sides (z/D =±1.0) compared to free jet data at two other jet Mach numbers: (a) M_j =0.75 and (b) M_j =1.055.

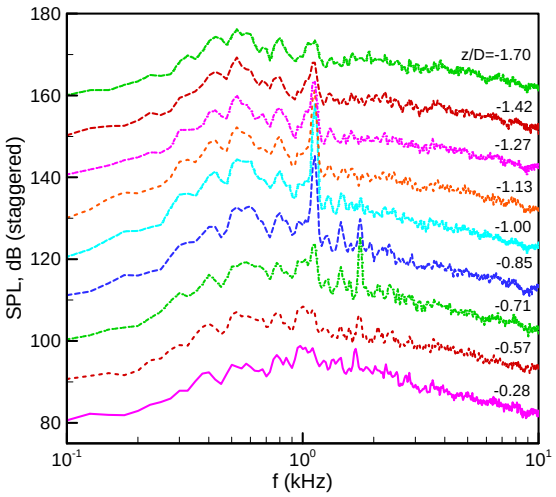

Fig. 14 SPL spectra on reflected side of plate for M_j =0.98, illustrating dependence of resonant tone on plate z/D; x_{TE}/D=5.66, θ=60˚.

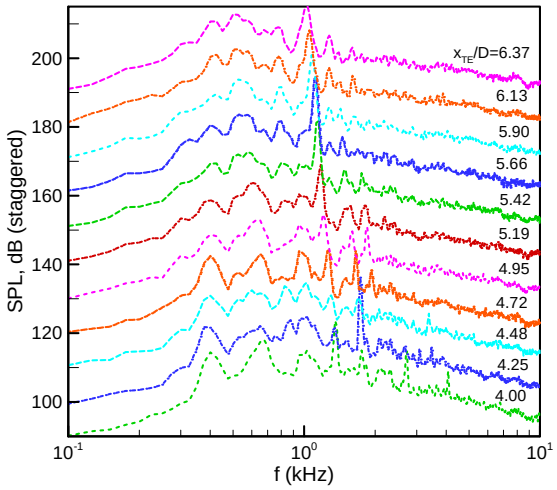

Fig. 16 SPL spectra on reflected side of plate for M_j =0.96, illustrating dependence of resonant tone on axial location of plate trailing edge x_{TE}/D; θ=60˚ (z/D varied in the range 0.71-1.15 to obtain maximum tone intensity at each x_{TE} location).

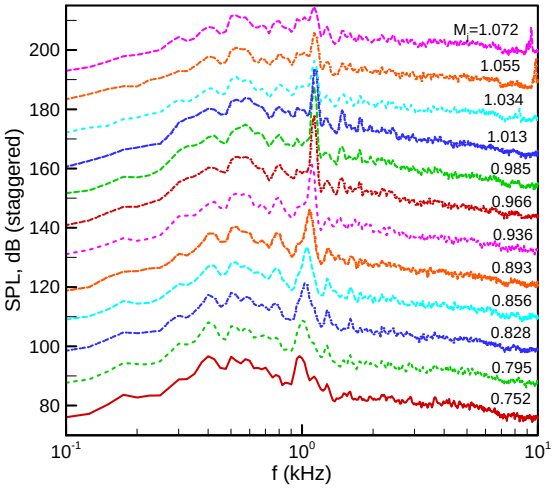

Fig. 15 SPL spectra on reflected side of plate for z/D= -1.00, illustrating dependence of resonant tone on M_j; x_{TE}/D=5.66, θ=60˚.

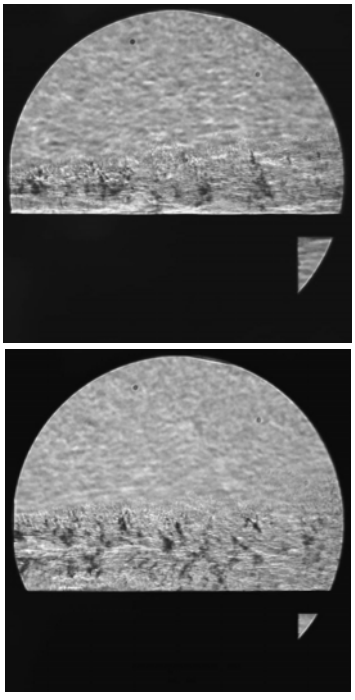

Fig. 17(a,b) Caption next page.

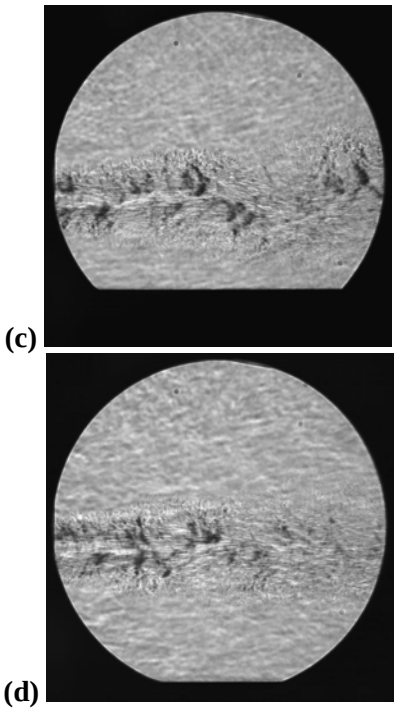

Fig. 17 Schlieren pictures of flowfield at M_j = 0.96 for x_{TE} /D = 5.66 with varying z: (a) z/D= -0.155 (lipline), (b) z/D= -0.50, (c) z/D= -1.00, (d) z/D= -1.50.

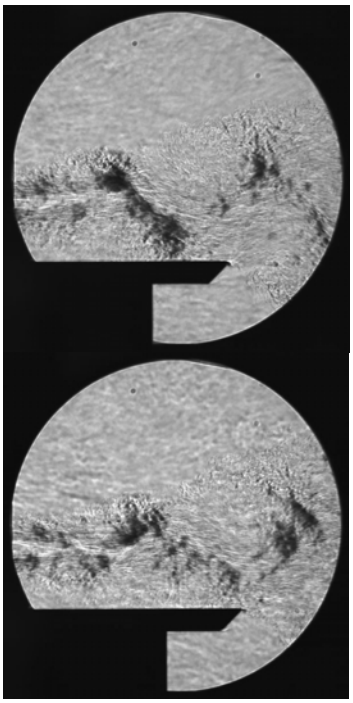

Fig. 18 Schlieren pictures of flowfield at M_j =0.96 for two cases when resonance was pronounced: (a) x_{TE} /D = 4.0, z/D=-0.71, (b) x_{TE} /D =4.25, z/D=-0.71.

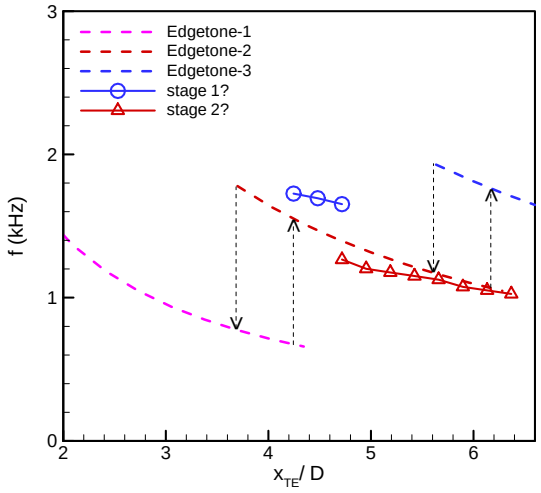

Fig. 19 Variation of tone frequency with plate trailing edge location. Dashed curves are for 'edgetone' frequency variation with location of leading edge of wedge, following equation given by Brown (1937); locations of stage jumps are drawn arbitrarily.